Cranial remains of *Ramsayia magna* from the Late Pleistocene of Australia and the evolution of gigantism in wombats (Marsupialia, Vombatidae)

by JULIEN LOUYS[1,*], MATHIEU DUVAL[1,2], ROBIN M. D. BECK[3], ELEANOR PEASE[4], IAN SOBBE[4,5], NOEL SANDS[6] *and* GILBERT J. PRICE[4]

[1]Australian Research Centre for Human Evolution (ARCHE), Griffith University, Brisbane, Queensland 4111, Australia; j.louys@griffith.edu.au
[2]Centro Nacional de Investigación sobre la Evolución Humana (CENIEH), Burgos 09002, Spain
[3]Ecosystems & Environment Research Centre, School of Science, Engineering & Environment, University of Salford, Manchester, UK
[4]School of Earth & Environmental Sciences, The University of Queensland, St Lucia, Queensland 4072, Australia
[5]Geosciences, Queensland Museum, Brisbane, Queensland 4011, Australia
[6]Central Queensland Speleological Society, Rockhampton, Queensland 4700, Australia
*Corresponding author

Typescript received 15 March 2022; accepted in revised form 1 September 2022

Abstract: Giant wombats (defined here as ≥70 kg) are found in the genera *Phascolonus*, *Ramsayia* and perhaps *Sedophascolomys*. *Ramsayia* is currently the most poorly known, having been described from mandibular and cranial fragments. Here, we report the most complete cranial remains attributable to the genus, identified as *R. magna*. The specimen provides new insights into the anatomy of the species and evolutionary adaptations to gigantism in Vombatidae. We record parietal sinuses in a vombatid for the first time, an adaptation to increased skull size relative to the braincase. The presence of a prominent premaxillary spine may indicate that the species possessed a large, fleshy nose. Both features are convergent on other large-bodied, non-vombatid extinct megaherbivores of Australia such as *Diprotodon optatum*. We use the cranial remains to examine the phylogenetic relationships of giant wombats to other vombatids. Phylogenetic analysis using maximum parsimony and Bayesian inference indicates that *Phascolomys*, *Ramsayia* and *Sedophascolomys* form a clade, suggesting a single origin of gigantism within Vombatidae. This origin may be related to the exploitation of poor-quality foods, and preceded extreme specializations observed in the cranial anatomy of the giant wombats. U-series and combined U-series and electron spin resonance (ESR) dating methods were applied to one fossil tooth. Age calculations systematically correlate the fossil remains to Marine Isotope Stage 5, and an age of *c.* 80 000 years can be proposed for this specimen. With only a single well-dated occurrence for this taxon, it is currently impossible to determine when and why *R. magna* became extinct.

Key words: megafauna, sinus, parietal, premaxillary spine, Pleistocene.

EXTINCT giant wombats of the family Vombatidae (broadly defined here as twice the size of modern wombats, i.e. having a body mass ≥*c.* 70 kg) are considerably rarer than the fossil diprotodontids (e.g. *Diprotodon*) that are often popularly (and incorrectly) referred as giant wombats. Large, isolated molars and maxillo-mandibular fragments referable to vombatids are sometimes found in Plio-Pleistocene fossil deposits (e.g. Archer 1976; Tedford & Wells 1990; Turnbull *et al.* 1990; Louys 2015; Hocknull *et al.* 2020). However, their usefulness in taxonomic and palaeobiological studies is usually restricted to genus-level classifications and stable isotope analyses, respectively, due to a general lack of species-level diagnostic features (e.g. McNamara 1990; De Santis *et al.* 2017). Giant vombatids belong to two or three described genera, the monotypic *Phascolonus* (species: *P. gigas*, *c.* 600 kg) and *Ramsayia* (species: *R. magna* and *R. lemleyi*, *c.* 100 kg), with the more diminutive (but still substantial) *Sedophascolomys* (species: *S. medius*, *c.* 70 kg) sometimes also referred to this group (see Beck *et al.* 2020 for body mass estimates). Of these, *P. gigas* is the best known. Originally described by Owen (1858), this species is the largest member of Vombatidae currently known and can be unambiguously distinguished from all other known vombatids by its broad, strap-like upper incisors (when these are preserved). Cranial remains of *P. gigas* are well represented in the Lake Callabonna deposits of South Australia (in particular, SAM P36279, casts of which are lodged in several museums), and are notable for the presence of a large depression in the frontals and parietals

doi: 10.1002/spp2.1475

(Murray 1998). Despite complete skulls having been available for study since the 1970s, to date description of the cranial anatomy of this species has been restricted to a brief general description by Murray (1998), and a more detailed study focused specifically on the basicranium by Tedford (2002).

Ramsayia has remained even more poorly known. *Ramsayia lemleyi* is restricted to the Pliocene of northwest and southeast Queensland (Archer 1976; Louys 2015); while a second species, *R. magna*, is more widely distributed in time and space, represented by putative specimens (*R.* sp. cf. *R. magna*) from the Pliocene deposits of Chinchilla, southeast Queensland and extending to the Plio-Pleistocene Bone Gulch Local Fauna, south central New South Wales (Tedford *et al.* 2006; Louys 2015). Despite having often been reported as restricted to the Late Pleistocene (e.g. Murray 1998; Johnson 2002), no doubt at least in part due to its recovery from the middle Late Pleistocene eastern Darling Downs deposits (Owen 1872; Dawson 1981), there have been no directly dated remains of *Ramsayia* reported in the literature. Price *et al.* (2009) reported U-series dates of *Macropus giganteus ?titan* teeth from Cement Mills, Gore, southeast Queensland, yielding minimum age constraints of 53.6 ± 0.2 and 53.9 ± 0.3 ka (2σ). This deposit also preserved fossils tentatively assigned to *R. magna*, suggesting that this species may have survived into the Late Pleistocene. *Ramsayia magna* is also poorly known anatomically, due to the fragmentary nature of fossils referable to the species and which consist of palatal, premaxillary and mandibular specimens only. As such, we have a very poor understanding of what this giant vombatid looked like, as well as its age, distribution and relationship with other vombatids.

In the early 2000s partially buried craniodental fragments of a large-bodied vombatid individual were found in a front chamber of Lower Johansons Cave, Rockhampton, Queensland by a combined Queensland University of Technology and Queensland Museum expedition. The specimen was originally reported as an undescribed genus and species of wombat (Hocknull 2009) but remained mostly buried at the time of initial assessment. Our later complete excavation and preparation of the material indicates that it can be referred to a species of *Ramsayia*. The specimen is hitherto the most complete individual known for the genus and, along with dating samples, has provided us with an opportunity to confirm the species diagnosis of *R. magna*, provide a detailed description of the cranial anatomy of this poorly known giant vombatid, and reassess its known geographical and temporal distribution. The specimen also enables us to examine the phylogenetic relationships of giant wombats and provide insights into adaptations associated with gigantism in this genus.

MATERIAL AND METHOD

The specimen was recovered from the rear of the front chamber of Lower Johansons Cave, Rockhampton, Queensland. It was found with mandible and cranium in articulation against the cave wall. Subsequent preparation by one of the authors (IS) showed that it was preserved in unconsolidated sediment unusually rich in microbat remains. It is curated in the palaeontological collections of the Queensland Museum (QM), under registration number QMF 60370. Body mass estimates were calculated using the TSL, 1LMW and 3LPW equations provided in the diprotodontians dataset of Myers (2001), using measurements listed below and applying the smearing estimate correction. As a point of comparison, body masses were also calculated for *Phascolonus gigas* and *Sedophascolomys medius* using the same equations with published measurements from Murray (1991*a*) and Louys (2015). 3D models of the skull were produced using standard turntable photogrammetry; full details are provided in Louys *et al.* (2022*a*) and Price (2022).

Geochronology

Samples and sample preparation. Electron spin resonance (ESR) and U–Th dating focused on a molar tooth of the individual. The burial sediments and adjacent limestone were sampled for dose rate evaluation (critical for ESR dating). Two samples (A and B) were collected from the tooth and prepared following the same procedure as in Duval *et al.* (2021): the enamel layer was mechanically separated from the other dental tissues, and both inner and outer surfaces were removed with a dentist drill to eliminate the volume that received an external alpha dose. The dentine and cement attached to the enamel layer were retained for subsequent solution bulk U-series analyses. All dental tissues were ground and sieved using a <200 μm mesh.

ESR dose evaluation. Dose evaluation used the multiple aliquot additive dose (MAAD) method. The enamel powder of each sample was split into 11 aliquots. Ten of them were gamma irradiated at the Centro Nacional de Investigación sobre la Evolución Humana (CENIEH; Spain) with a Gammacell 1000 Cs-137 gamma source (dose rate, 6.27 ± 0.14 Gy/min) to the following doses: 49.0, 98.1, 147.0, 196.0, 294.1, 392.1, 588.0, 784.0, 980.0 and 1960.0 Gy. One aliquot was kept unirradiated (as the natural aliquot).

Room temperature ESR measurements were carried out at CENIEH with an EMXmicro 6/1 Bruker ESR spectrometer coupled to a standard rectangular ER 4102ST cavity. The following procedure was used to minimize

analytical uncertainties: (1) all aliquots of a given sample were carefully weighed into their corresponding tubes and a variation of <1 mg was tolerated between aliquots; and (2) ESR measurements were performed using a Teflon sample tube holder inserted from the bottom of the cavity to ensure that the vertical position of the tubes remains exactly the same for all aliquots. The following acquisition parameters were used: 1–60 scans, 1 mW microwave power, 1024 point resolution, 15 mT sweep width, 100 kHz modulation frequency, 0.1 mT modulation amplitude, 20 ms conversion time and 5 ms time constant. All aliquots of a given sample were measured within a short time interval (<1 h). This procedure was repeated three times over successive days without removing the enamel from the ESR tubes between measurements in order to evaluate measurement and equivalent dose (D_E) precisions (Table 1).

The ESR intensities were extracted from T1–B2 peak-to-peak amplitudes of the ESR signal (Grün 2000) and then normalized to the corresponding number of scans and aliquot mass. D_E values were obtained by fitting a single saturating exponential through the mean ESR intensities derived from the repeated measurements. Fitting was performed with Microcal OriginPro 9.1, which is based on a Levenberg–Marquardt algorithm by chi-square minimization. Data were weighted by the inverse of the squared ESR intensity ($1/I^2$) and the inverse of the squared experimental errors ($1/s^2$). ESR dose–response curves are shown in Figure 1. The final 1σ D_E error used for age calculation (Table 1) includes both the fitting and gamma source dose rate errors.

U-series analyses of dental tissues. Powdered enamel and dentine samples were weighed and then spiked using a ^{229}Th–^{233}U tracer before being digested in concentrated HNO_3. The solutions were then treated with H_2O_2 to remove trace organics, with U and Th then separated using conventional column chemistry techniques as described in Price *et al.* (2013) and Clark *et al.* (2014). Both U and Th were collected into the same pre-cleaned test tube using 3 mL 2% HNO_3 mixed with a trace amount of HF. U–Th isotopic ratios were then measured using a Nu Instruments Plasma multicollector–inductively coupled plasma mass spectrometer (MC-ICP-MS) in the Radiogenic Isotope Facility at The University of Queensland, Brisbane, Australia, following analytical protocols established by Zhao *et al.* (2009). U-series results are listed in Table 2.

Dose rate evaluation and age calculations. No *in situ* evaluation of the gamma dose rate associated with the teeth was performed in the field. Consequently, both the beta and gamma dose rates were derived from laboratory analysis of the six bulk samples extracted from the surrounding sediment and cave wall that were collected on site. The ICP-MS analyses were performed by Genalysis Laboratory Services following a four-acid digest preparation procedure. Radioelement concentrations (U, Th and K) are given in Table 3.

The following parameters were used for the dose rate calculations: an alpha efficiency of 0.13 ± 0.02 (Grün & Katzenberger-Apel 1994), Monte-Carlo beta attenuation

TABLE 1. Detailed ESR results obtained for the two fossil teeth.

Sample	535A	535B
Average weight per aliquot (mg)	11.1 ± 0.3	10.9 ± 0.5
Number of repeated measurements	3	3
Measurement precision* (%)	1.5	0.9
SSE fitting (data weighting by 1/I†)		
Non-corrected ESR intensities		
DE precision† (%)	6.5	8.3
Adj. *r*-squared	0.999	0.999
D_{E1} (Gy)	34.9 ± 1.0	39.8 ± 1.3
D_{max} (Gy)	1960	1960
D_{max}/D_{E1}	56.1	49.3
Adj. *r*-squared	0.999	0.998
D_{E2} (Gy)	35.0 ± 2.4	41.1 ± 3.1
D_{max} (Gy)	294	294
D_{max}/D_{E2}	8.4	7.2
Baseline-corrected ESR intensities		
Adj. *r*-squared	0.999	0.999
D_{E3} (Gy)	32.3 ± 1.0	38.9 ± 2.7
D_{max} (Gy)	294	294
D_{max}/D_{E3}	9.1	7.6
Noise-subtracted ESR intensities		
Adj. *r*-squared	0.999	0.994
D_{E4} (Gy)	30.0 ± 2.0	38.2 ± 4.9
D_{max} (Gy)	294	294
D_{max}/D_{E4}	9.8	7.7
SSE fitting (data weighting by 1/s†)		
Noise-subtracted ESR intensities		
Adj. *r*-squared	0.991	0.991
D_{E5} (Gy)	28.0 ± 2.6	34.7 ± 15.5
D_{max} (Gy)	294	294
D_{max}/D_{E5}	10.5	8.5
D_E ratios		
D_{E2}/D_{E1} ratio	1.00	1.03
D_{E3}/D_{E2} ratio	0.92	0.95
D_{E4}/D_{E3} ratio	0.93	0.98
D_{E5}/D_{E4} ratio	0.96	0.91

*Measurement precision is expressed as the mean coefficient of variation obtained for all of the aliquots of a given sample after the three repeated measurements.

†D_E precision is the variation of the D_E values derived from the repeated measurements of a given sample (derived from the non-corrected ESR intensities).

D_E, equivalent dose; ESR, electron spin resonance; SSE, single saturating exponential.

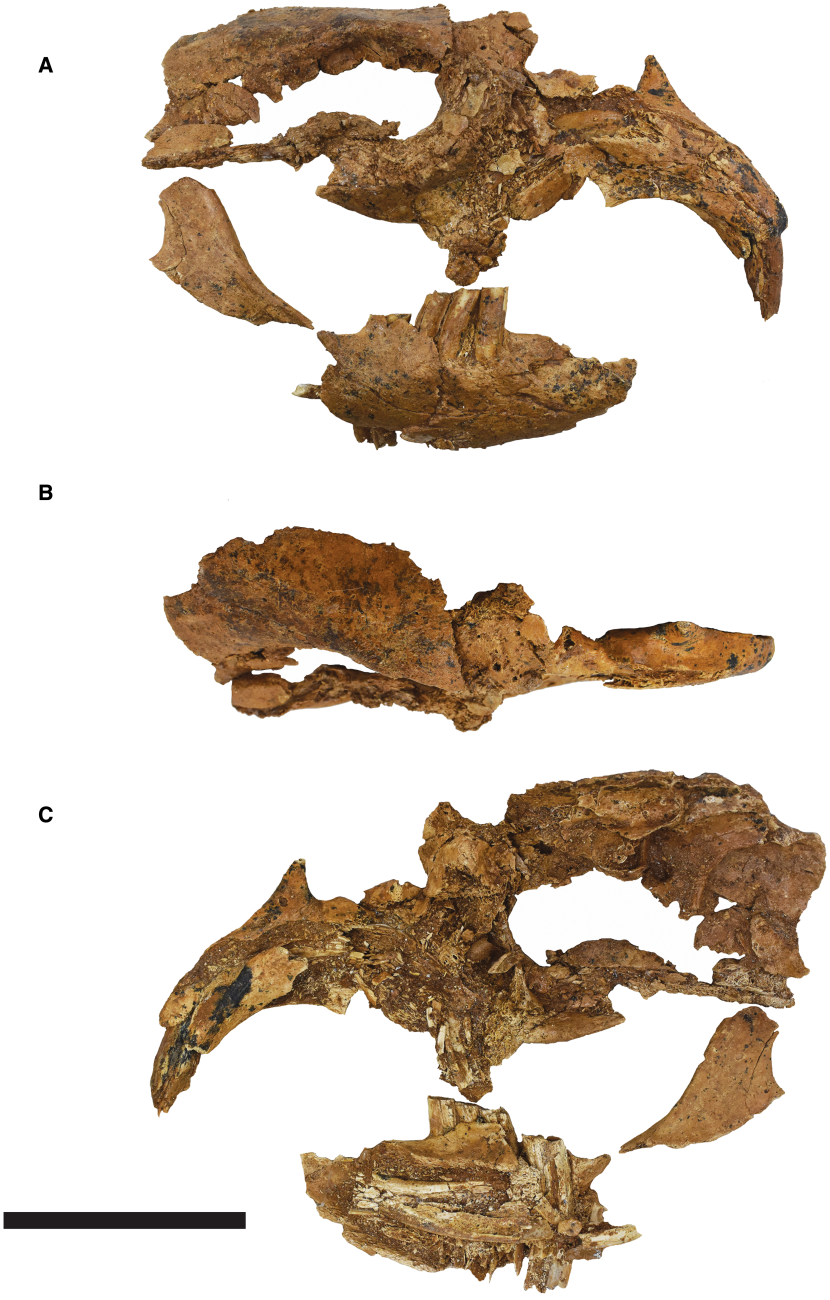

FIG. 1. QMF 60370, a partially preserved cranium and articulated mandible of *Ramsayia magna* from Lower Johansons Cave, Rockhampton, Queensland. A, lateral; B, dorsal; C, endocranial view. Scale bar represents 100 mm.

factors from Marsh (1999), dose rate conversion factors from Guérin *et al.* (2011), and an assumed long-term water content value (% wet weight) of 0%, 5 ± 3%, 15 ± 5% and 0% in enamel, dentine and cement, sediment, and limestone, respectively. Post-Rn equilibrium was assumed in dental tissues and sediment. A cosmic dose rate of 30 ± 10 μGy/a was estimated by talking into account the distance of the fossil specimen from the entrance (*c.* 100 m) and the thickness of the overburden limestone (estimated >20 m). Given the existing uncertainty on these estimates, a relatively large 1σ relative error (33%) was used. Initial beta and gamma dose rate evaluations were performed using a tooth geometry of cement/enamel/dentine and considering a 50/50 contribution from the sediment and the cave wall, respectively.

Age calculations were performed with USESR, a Matlab-based program (Shao *et al.* 2014) using the uranium series (US) and accelerating uptake (AU) models defined by Grün *et al.* (1988) and Shao *et al.* (2012), respectively. Usually the US model is preferred, except in the case of dental tissues showing apparent uranium leaching, when the AU model would be used instead.

TABLE 2. U-series data obtained from solution ICP-MS analyses of the powdered dental tissues.

Sample ID	Tissue	U (ppm)*	$^{230}Th/^{232}Th$*	$^{230}Th/^{238}U$*	$^{234}U/^{238}U$	Uncorrected ^{230}Th age (ka)*	Corrected ^{230}Th age (ka)*	Corrected initial $(^{234}U/^{238}U)$*
535A	Dentine	0.1260 ± 0.0003	46.37 ± 0.75	1.0130 ± 0.0160	2.1311 ± 0.0033	66.0 ± 1.4	65.1 ± 1.4	2.3843 ± 0.0127
	Enamel	0.0926 ± 0.0005	121.2 ± 2.3	1.0278 ± 0.0198	1.4963 ± 0.0071	115.9 ± 3.8	115.4 ± 3.8	1.6923 ± 0.0110
535B	Cement	0.2257 ± 0.0049	4.77 ± 0.09	0.9173 ± 0.0228	2.057 ± 0.034	60.9 ± 2.3	52.9 ± 4.3	2.4580 ± 0.1305
	Dentine	0.1149 ± 0.0003	16.90 ± 0.21	0.7801 ± 0.0095	2.0221 ± 0.0034	50.9 ± 0.8	48.9 ± 1.0	2.2199 ± 0.0225
	Enamel	0.1703 ± 0.0008	216.9 ± 2.6	1.1566 ± 0.0144	1.1910 ± 0.0056	284 ± 16	284 ± 16	1.4273 ± 0.0184

*Errors are 2σ.
ICP-MS, inductively coupled plasma mass spectrometer.

Additional ages were calculated using the early uptake (EU) and linear uptake (LU) models for comparison. These last two calculations were performed using DATA (Grün 2009). Data inputs and outputs are given in Table 4. Age results are given at the 1σ confidence level.

Phylogenetics

To examine the information provided by QMF 60370 on the phylogenetic relationships of *Ramsayia magna*, we used a revised version of the morphological character matrix of Beck *et al.* (2020), which was developed to resolve relationships within Vombatiformes. This matrix consists of 79 craniodental and 20 postcranial characters, to which we added one additional craniodental character, namely presence or absence of a strongly arched bony palate (Louys *et al.* 2022*b*). The palate is strongly arched in *Ramsayia magna* (Dawson 1983), *Sedophascolomys medius* (Louys 2015) and *Phasolonus gigas* (Dawson 1983), with the bony palate steeply sided immediately medial to the molars, before curving horizontally more medially to form an overall arched shape; Tedford (2002) referred to this morphology as an 'emarginated palate'. Tedford (2002, table 1) stated that an arched (emarginated) palate is present in *Lasiorhinus* (as well as '*Phascolomys*' [= *Sedophascolomys*] *medius* and *Phascolonus gigas*), but the accompanying text and figure 7 suggest that this is an error, and our own examination of multiple specimens of both *Lasiorhinus* species confirms that the palate is not strongly arched in this taxon. We used QMF 60370 to revise and add to the scorings of *Ramsayia magna*; as a result, *R. magna* could be scored for 36 out of the 100 characters (36% complete). In the final matrix, 86 of the 100 characters were parsimony informative, and the remaining 14 (i.e. 14%) autapomorphic.

Following Beck *et al.* (2020), the final morphological matrix was analysed using maximum parsimony and undated Bayesian analysis, with 15 characters representing putative morphoclines specified as ordered, and the didelphimorphian *Didelphis marsupialis* used as the outgroup taxon. Maximum parsimony analysis was carried out using PAUP* 4.0a169, with variable character scorings treated differently depending on whether they reflected scoring uncertainty ('either/or') or polymorphism, using the 'mstaxa=variable' command. The tree search used a two-stage strategy, with 1000 random addition replicates with TBR (tree bisection and reconnection) branch swapping, saving 10 trees per replicate, followed by a heuristic search in the initial set of saved trees. All branches in the final set of saved trees that had a minimum branch length of zero were collapsed (using the 'condense collapse=minbrlen' command), and the remaining trees were then summarized using strict consensus. Support values were

TABLE 3. Radioelement concentrations measured in the raw sediment and limestone samples.

Sample ID	Type	U (ppm)	Th (ppm)	K (%)
A	Sediment	1.30 ± 0.08	6.40 ± 0.27	0.85 ± 0.03
B	Sediment	1.29 ± 0.08	6.39 ± 0.27	0.87 ± 0.03
C	Sediment	1.28 ± 0.08	6.43 ± 0.27	0.85 ± 0.03
D	Limestone	0.31 ± 0.07	1.26 ± 0.07	0.12 ± 0.01
E	Limestone	0.08 ± 0.07	0.25 ± 0.05	0.05 ± 0.00
F	Limestone	0.08 ± 0.07	0.27 ± 0.07	0.06 ± 0.00
Mean* (A, B, C) ± 1 SD (cv)	Sediment	1.29 ± 0.01 (0.8%)	6.41 ± 0.02 (0.3%)	0.85 ± 0.01 (1.1%)
Mean* (E, F) ± 1 SD (cv)	Limestone	0.08 ± 0.00 (0.0%)	0.26 ± 0.01 (5.4%)	0.06 ± 0.00 (6.9%)

*cv, coefficient of variation; SD, standard deviation. The mean value calculated for the limestone samples was taken from samples E and F (see text for explanation).

TABLE 4. Data inputs and outputs associated with the combined U-series–ESR age calculations.

Sample	535A	535B
Enamel		
Dose (Gy)	30.0 ± 2.2	38.2 ± 5.0
U (ppm), $^{234}U/^{238}U$, $^{230}Th/^{234}U$	See Table 2	See Table 2
Alpha efficiency*	0.13 ± 0.02	0.13 ± 0.02
Water content (%)	0	0
Initial enamel thickness (μm)†	744 ± 74	1181 ± 118
Dentine		
U (ppm), $^{234}U/^{238}U$, $^{230}Th/^{234}U$	See Table 2	See Table 2
Water (%)	5 ± 3	5 ± 3
Removed enamel thickness (μm)†	97 ± 10	47 ± 5
Sediment		
U (ppm), Th (ppm), K (ppm)	See Table 3	See Table 3
Water (%)	15 ± 5	15 ± 5
Removed thickness (μm)†	93 ± 9	107 ± 11
AU-ESR age calculations (cement thickness >2 mm)§		
Internal dose rate (μGy/a)	31 ± 1	39 ± 6
Beta dose rate, dentine (μGy/a)	2 ± 1	1 ± 0
Beta dose rate, cement (μGy/a)	3 ± 0	4 ± 1
Gamma + cosmic dose rate (μGy/a)	322 ± 18	322 ± 18
Total dose rate (μGy/a)	358 ± 18	366 ± 16
AU-ESR age (ka)	84 ± 6	105 ± 12
EU-ESR age (ka)¶	85 ± 9	102 ± 15
LU-ESR age (ka)¶	90 ± 10	111 ± 17
AU-ESR age calculations (cement thickness = 0.3 mm)§		
Internal dose rate (μGy/a)	33 ± 1	33 ± 8
Beta dose rate, dentine (μGy/a)	2 ± 0	1 ± 0
Beta dose rate, cement (μGy/a)	66 ± 6	63 ± 5
Gamma + cosmic dose rate (μGy/a)	322 ± 18	322 ± 18
Total dose rate (μGy/a)	423 ± 18	417 ± 42
AU-ESR age (ka)	71 ± 5	92 ± 10

*From Grün & Katzenberger-Apel (1994).
†A 10% error was assumed.
§All errors are given at a 1σ confidence level.
¶EU-ESR and LU-ESR age estimates are given for comparison only, to illustrate the limited impact of uranium modelling on the results.
AU, accelerating uptake; ESR, electron spin resonance; EU, early uptake; LU, linear uptake.

then calculated on the strict consensus using bootstrapping, with 2000 standard heuristic bootstrap replicates, saving a maximum of 1000 trees per replicate.

Undated Bayesian analysis was carried out using MrBayes 3.2.7. Because the matrix included a relatively large proportion (14/100, i.e. 14%) of autapomorphies, we used the Markov variable (Mk*v*) variant of the Lewis (2001) model as our substitution model, which assumes that variable characters (rather than simply parsimony-informative characters) have been scored. Rate heterogeneity between characters was modelled as a lognormal distribution with eight rate categories, following Harrison & Larsson (2015). The MrBayes analysis consists of four independent runs of four MCMC chains, using default heating and temperature parameters, run for 10 million generations, and sampling of trees and other parameters every 5000 generations. Plots of parameters in Tracer indicated that stationarity and convergence between runs was achieved within the first 2.5 million generations (i.e. 25%), and hence the trees from the remaining 7.5 million generations were summarized using 50% majority rule consensus (as recommended by O'Reilly & Donoghue 2018), giving support values as Bayesian posterior probabilities (BPPs).

SYSTEMATIC PALAEONTOLOGY

Order DIPROTODONTIA Owen, 1866 *sensu* Beck *et al.* (2020, table 1)
Suborder VOMBATIFORMES Woodburne, 1984 *sensu* Beck *et al.* (2020, table 1)
Superfamily VOMBATOIDEA Kirsch, 1968 *sensu* Beck *et al.* (2020, table 1)
Family VOMBATIDAE Burnett, 1830
Ramsayia magna (Owen, 1872)

Material. QMF 60370, a partially preserved cranium and articulated mandible. Teeth preserved include right upper and lower

incisor (latter only partially preserved root in incisor alveoli), right p3, m1–2, partial M1, M?3–4. The cranium has minimum length of 291.5 mm and preserves aspects of the premaxilla, maxilla, nasals, frontal and parietal (Figs 1–3; 3D models provided in: Appendix S1; Louys *et al.* 2022*a*; Price 2022).

Description

We focus on those aspects of the cranial anatomy of the species that have not been described in previous works (Dawson 1981, Louys 2015). Brief, taxonomically pertinent descriptions of the teeth are also presented. For previous descriptions of the anatomy of the species, especially dental anatomy, readers are referred to Dawson (1981), Murray (1998) and Louys (2015). Postcanine dental dimensions are given in Table 5.

Premaxilla. Right lateral view. The premaxilla is strongly curved, almost circular, and closely surrounds the upper first incisor. Only the anterior portion of the premaxilla is preserved; where it is broken towards the orbit, the root of the upper first incisor is exposed. This tooth extends at least as far as the orbit and the fragments of a badly damaged P3. The dorsal surface of the premaxilla is flat and follows the curvature of I1 for *c.* 71 mm, before curving steeply dorsally and forming a distinct premaxillary spine (i.e. the median premaxillary process). This spine extends at least 16 mm above the roof of the main body of the premaxilla. While the anterior aspect of the process is steeply angled (*c.* 75°), the posterior aspect is sheer: it forms an almost 90° angle with the roof of the main body of the premaxilla.

Interior medial view. The right premaxilla forms a closed sheath around the first incisor. The mediolateral width of this bone is 22.5 mm. There is no evidence for any synostosis between left and right premaxillae. The anteromedial part of the premaxilla is flat, while the ventral surface twists dorsomedially. The anteromedial flatness of the premaxilla extends to the premaxillary spine. Posterior to the spine, the premaxilla domes slightly dorsally, forming a slight bump in the bone. The premaxilla is not preserved posteriorly beyond this bump; however, the posterior margin is reminiscent of a suture and we interpret this as the anatomical limit of the bone. No evidence of an incisive foramen is preserved in this specimen.

First upper incisor. This tooth is transversely narrow, thick, long and strongly curved. Enamel is restricted to the dorsal surface with an ovate, vertical wear facet on the lingual surface. The exposed tooth measures 17 mm (anteroposterior length) by 15.5 mm (mediolateral width).

Nasal. Right lateral view. The nasal is preserved as a rectangular fragment, bounded ventrally and posteriorly by the maxilla. In anterior view the ventral extent of the nasal forms a sharp wedge. The dorsal part of the nasal is not preserved; however, it is probably broken at the dorsal extent of the nasomaxillary suture. If this is correct, this suture is orientated anteroposteriorly, ending where it meets the frontal and reaching *c.* 17.5 mm in length; thus, the nasal formed a rostrolaterally oriented suture with the frontals.

Interior medial view. The nasal is preserved only as an anteromedially facing bone that is relatively flat, although the most ventral aspect preserved appears to be angled horizontally. The maximum width of the preserved nasal is *c.* 37 mm. A faint nasomaxillary suture is visible: it extends medioventrally at a *c.* 45° angle.

Maxilla. The maxilla is preserved in two regions. The maxilla ascending process (*sensu* Trusler & Sharp 2016) is adjacent to a pyramid-shaped fragment at the posterior extent of the dorsal surface of the maxilla. A very weak process oriented posteromedially and forming a distinct side of the pyramid is visible. The relationship between this fragment and the nasal is not preserved. Dorsoposterior to this fragment is the maxilla ascending process, which is also poorly preserved: only a rectangular fragment of this process remains. This process nevertheless contacts the frontal with a straight, rostrolateral suture. The body of the maxilla is poorly preserved.

Above the postcanine toothrow, the maxilla is moderately well preserved. The anterior margin of the anterior root of the zygomatic arch is positioned above the fragmentary remains of the P3. The anterior root extends posteriorly to approximately level with the M2. The infraorbital fossa, where the superficial masseter originates in modern wombats (Kupczik *et al.* 2015), is weakly developed: the zygomatic arch forms an almost 90° angle with the dental arcade, and it juts out at least 23 mm. Posterior to the anterior zygomatic root, the remainder of the preserved maxilla bulges slightly and curves posteriorly.

Frontal. The frontal is preserved as a dorsally flattened bone. It is preserved from its contact with the maxilla, anteriorly, to its contact with the parietal, posteriorly; the latter contact takes the form of a strongly anterolateral angled suture. The bone has a well-developed, thickened frontoparietal crest, which forms a shelf above the attachment for the temporalis muscle. A deep frontal fossa is positioned just anterior to the frontoparietal suture; this suture marks the posterior extent of the postorbital process. Anteriorly, the frontoparietal crest ends at a weakly developed postorbital process.

Parietal. This bone is preserved only as a triangular fragment at the rear of the skull. Where it contacts the frontal laterally, it marks the end of the frontoparietal crest. This point also marks the narrowest part of the dorsal surface of the skull; in this sense it is relatively broad: broader than *Lasiorhinus* and *Vombatus*, but more reminiscent of *Lasiorhinus*, which has a wider parietal than *Vombatus* (see Scott *et al.* 1988, fig. 2). It shows no evidence of the concave, 'dished-in' dorsal surface (Murray 1998) seen in *Phascolonus*.

Squamosal and jugal. These bones are very poorly preserved but together they define the posterior extent of the zygomatic arch. Their contact with the parietal or maxilla or each other is too heavily damaged to be discerned.

Sinuses. Posterior to the maxilla, a poorly preserved frontal sinus is present. It measures 23 mm long and 15 mm at maximum width (at its anterior extent). In the parietal, three large

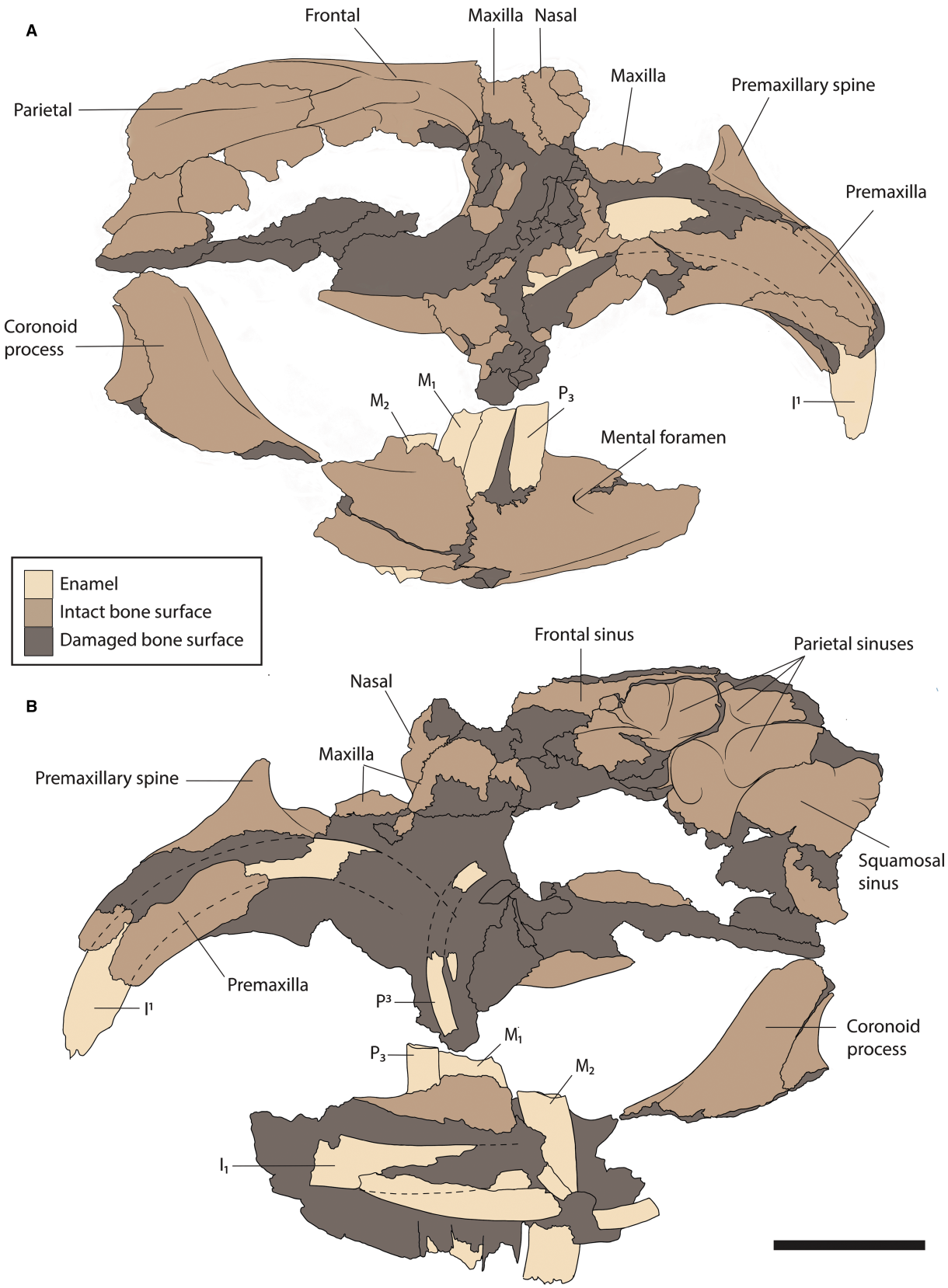

FIG. 2. Line drawing and anatomical interpretation of QMF 60370. Enamel indicated in light brown, intact bone surface in moderate brown, and damaged/highly fragmented bone in dark brown. A, lateral; B, endocranial view. Scale bar represents 50 mm.

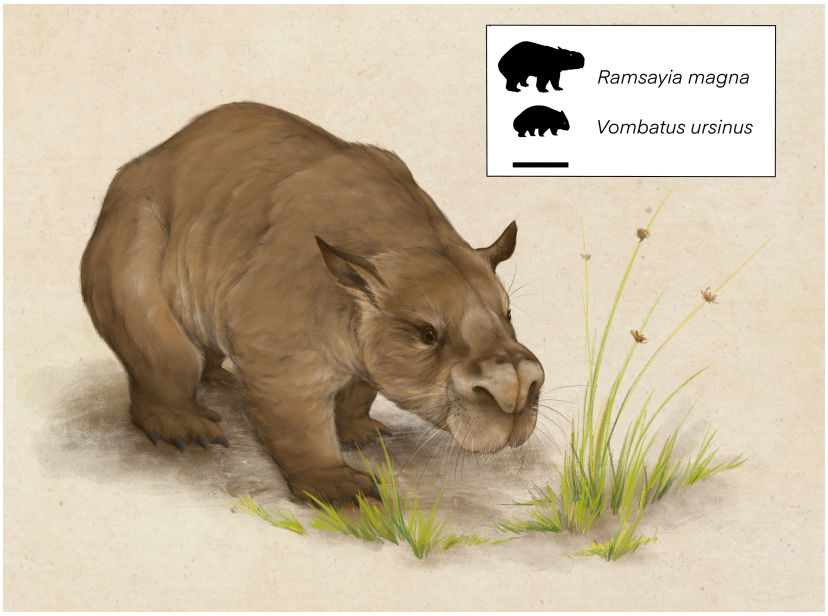

FIG. 3. Life reconstruction of *Ramsayia magna*. Silhouette shown in relation to the modern common wombat, *Vombatus ursinus*. Scale bar represents 1 m. Illustration by Eleanor Pease.

TABLE 5. Postcanine dental metrics (in mm) from QMF 60370, *Ramsayia magna*.

Tooth	Width (anterior/ posterior loph)	Length	Height
M?3	11.17/broken	20.39	Broken
M?4	8.94/7.12	14.76	Broken
p3	8.56	11.53	70.32
m1	11.31/11.21	21.92	74.20
m2	Broken	Broken	63.86

sinuses are present: an anterior sinus that is well defined at its dorsal surface but broken ventrally and separated from the others by a large trabecula; and two posterior sinuses that are poorly separated, with the larger positioned dorsal to the smaller. The smaller, ventral sinus is deeper, however, and extends anterolaterally. These posterior parietal sinuses are clearly separated from what we interpret to be a large squamosal sinus by another trabecula. This last sinus is incomplete but is the largest preserved: 42 mm in length and 50 mm in height; it probably represents the dorsal part of the posterior epitympanic sinus that is present in other vombatids and most other diprotodontians (Beck *et al.* 2022).

Mandible. Lateral view. The mandible is preserved from *c.* 57 mm anterior to p3 to the anterior root of the ascending ramus. The body of the mandible is robust, deepening posteriorly to the level of the p3–m1. Only a single mental foramen appears to have been present, as in other vombatids (Beck *et al.* 2022, char. 98): it forms a deep sulcus in the mandible *c.* 15.5 mm below the toothrow and 13.5 mm anterior to p3. The root of the ascending ramus begins at the level of the m3 alveolus.

Medial view. The mandible is largely broken, and it has exposed part of the lower incisor. This tooth, preserved only in the socket, narrows anteriorly before being broken. This anterior narrowing could be the result of post-depositional damage because the tooth is preserved in two broad fragments, with the dorsal fragment potentially having been displaced anterodorsally relative to the more ventral fragment (Fig. 2). The medial surface of the mandible, where preserved, is strongly dorsoventrally inclined, almost vertical, for at least 19 mm below the level of the m1; no symphysis is preserved in this specimen. The p3 is subrounded and triangular. Where preserved, the m1–2 exhibit rounded borders and broad, V-shaped median valleys.

The coronoid process of the mandible is also preserved as a separate fragment, with the anterior part of the mandibular notch present. This notch extends 23 mm ventrally. The coronoid process thickens ventrally, forming a shelf towards the molar row, from 5.5 mm thick at the dorsal extent to 9.2 mm at its ventrally preserved margin.

Remarks

This specimen (QMF 60370) can be referred to *Ramsayia* based on its combination of large size (roughly three times larger than *Vombatus ursinus*), anterior–posterior length of the upper incisor only just exceeding the medial–lateral width (ratio of 10:11); upper incisor elongate and strongly curved, with ovate vertical wear facet on lingual surface; diastema deeply concave; lower incisor with dentine exposure restricted to dorsal surface; subrounded triangular p3; and lower molars with rounded borders and broad, V-shaped median valleys (Dawson 1981, 1983; Murray 1998; Louys 2015). It is referred to *R. magna* rather than *R. lemleyi* based on its less elongate p3 (length 11.5 mm vs 18.5 mm in *R. lemleyi* holotype; Archer 1976), which also lacks any evidence of a medial lingual groove (Archer 1976).

To this we can add additional details of differences between *R. magna* and the only other known member of the genus, *R. lemleyi*. *Ramsayia magna* differs from *R. lemleyi* in possessing a p3 with length much shorter than m1 (p3:m1 *c.* 0.5 in our specimen compared with *c.* 0.85 in *R. lemleyi*, as reported in Archer 1976). A dorsoventrally extended i1 root compared with its crown in our specimen might also distinguish *R. magna* from *R. lemleyi*; however, we cannot rule out the possibility that this is an artefact of poor preservation of the mandible, and further *R. magna* specimens will be required to confirm whether it is a genuine feature of this species. Such a feature would be markedly different to the morphology of ever-growing incisors seen in other wombats, in which the lower incisor dorsoventral length is fairly consistent along the axis of the tooth and its continuous growth an adaptation to high rates of wear.

Ramsayia magna was erected by Dawson (1981) based on material previously described as *Phascolomys magnus* Owen, 1872. *Phascolomys magnus* had already been erected by Murie (1866) based on a mandibular fragment, tibia, ulna, radius, several vertebrae and other fragmentary bones from Eton Vale in the eastern Darling Downs (Mahoney & Ride 1975). Mahoney & Ride (1975) attempted to locate the specimens assigned to this species by Murie (1866) in the British Museum (Natural History), but they were insufficiently satisfied with the provenance data associated with the specimens matching the descriptions provided by Murie (1866) to positively identify the syntypes. The most likely match for the mandibular fragment, as identified by Mahoney & Ride (1975) was figured and described as *Phascolonus gigas* by Owen (1872). Although Mahoney & Ride (1975) suggested that *Phascolomys magnus* Murie, 1866 is probably a junior synonym of *Phascolonus gigas* (Owen, 1858), they did not go so far as formally synonymizing it. Thus, *Phascolomys magnus* Murie, 1866 has remained a valid taxon name but with no defined types. The name also has priority and is the primary homonym of *Phascolomys magnus* Owen, 1872, which was not an available name when published; the species was only formally fixed by Dawson (1981) when she established *Ramsayia magna* and assigned *Phascolomys magnus* Owen, 1872 to the genus. To reduce any further ambiguity, here we consider *Phascolomys magnus* Murie, 1866 a *nomen dubium*. We do so because the syntypes have not been positively identified, and it is not possible to assign it to any valid vombatid species based on the published description by Murie (1866) (although it is almost certainly *Phascolonus gigas* based on the later description by Owen 1872).

RESULTS

Body mass

Body mass estimates were 180 kg (TSL; raw estimate 172 kg), 143 kg (1LMW; raw estimate 120 kg), and 59 kg (3LPW; raw estimate 44 kg). The average of the estimates is 128 kg; however, because the total skull length is not preserved (and the measurement a minimum), this is likely to represent a minimum estimate of the body mass of *R. magna*. In comparison, the body mass average for *Sedophascolomys medius* was 75 kg (mean of 3LPW for QMF845, and 1LMW for QMF845 and QMF56218; raw measurements from Louys 2015), and for *Phascolonus gigas* it was 361 kg (mean of 1LMW for QMF56219 and QMF821, and TSL of *P. gigas*; raw values from Louys 2015 and Murray 1991*a*, table 16).

Geochronology

ESR dose evaluation. Measurement precision achieved is excellent, with all samples showing a variation of 0.9–1.5% (Table 1). This results in a reasonably good D_E repeatability of between 5 and 10%. The D_E values obtained over the full irradiation dose range are *c.* 35 and 40 Gy for samples A and B, respectively (D_{E1} values in Table 1; Fig. 4). Given that the corresponding D_{max}/D_E ratios are significantly higher than the range recommended by Duval & Grün (2016) ($5 < D_{max}/D_E < 10$) for D_E values of this magnitude (<100 Gy), additional dose–response curve fitting was performed after adjusting the maximum applied irradiation dose (D_{max}) to 294 Gy. This operation has, however, only a very limited impact on the D_E estimates (D_{E2} values in Table 1), which become slightly higher by 0–3%. They remain systematically 1σ consistent with the values initially obtained, although the relative D_E errors increase by a factor of >2.

Given the limited amount of material available for the ESR measurements (aliquots of *c.* 11 mg each; Table 1) and the small D_E values (<50 Gy), the two enamel samples A and B are characterized by relatively weak ESR intensities. To achieve an acceptable low signal-to-noise (S/N) ratio, acquisitions of up to 60 scans for the least irradiated aliquots have been performed, resulting in S/N values of 8–10 for the natural aliquots. Despite these conditions, several ESR spectra show non-horizontal baseline and non-negligible high-frequency noise, both of which may significantly bias the D_E evaluation if not taken into account. Consequently, a cubic baseline correction was systematically applied to all ESR spectra as in Duval & Martín-Francés (2017) before extracting the T1–B2 ESR intensity. Additionally, the mean scan-normalized noise ESR intensity extracted from all of the aliquots of a given sample measured at a given time was subtracted from the intensity of the radiation-induced ESR signals. D_E evaluation was performed using the baseline-corrected and noise-subtracted ESR intensities, yielding the D_{E3} and D_{E4} values given in Table 1. D_{E3} values are 5–8% lower than D_{E2} values, while D_E4 values are even lower by an additional 2–7% depending on the sample considered. Basically, these corrections have virtually no impact on the resulting D_E values for sample B (<2 Gy), whereas sample A is more affected (5 Gy). Age calculations are based on D_{E4} values (Fig. 4). Finally, an additional fitting was

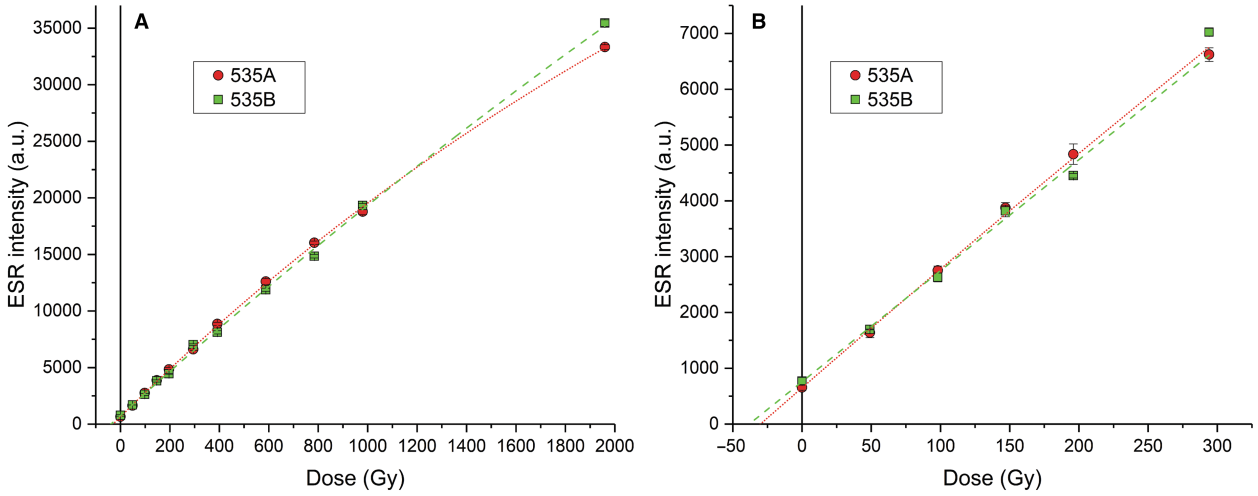

FIG. 4. Electron spin resonance (ESR) dose–response curves obtained for the two tooth enamel samples 535A and 535B. The ESR intensities and associated errors of each aliquot correspond to the mean value and 1 standard deviation derived from the repeated ESR measurements. A, non-corrected ESR intensities (D_{max} = 1960 Gy; D_{E1}). B, baseline-corrected and noise-subtracted ESR intensities (D_{max} = 294 Gy; D_{E4}).

performed using data weighting by $1/s^2$: the resulting D_{E5} values become lower than D_{E4}, although all values remain within the 1σ error: –2 Gy for sample A, and –3.5 Gy for sample B, although the significance of the latter should be considered with caution given the large D_{E5} error (15.5 Gy). These results illustrate the limited impact of data weighting on the fitting outcome.

Solution U-series analyses. Solution U-series analyses of the bulk powdered dental tissues show that: (1) the enamel tissues have very low uranium concentrations (<0.5 ppm); and (2) there is no apparent evidence of uranium leaching in any of the samples (i.e. a finite age can be obtained for all samples). These two observations indicate that the samples are suitable for ESR dating.

Apparent U-series age estimates range from *c.* 49 to 284 ka (Table 2). No significant detrital Th contamination is observed in the samples, thus resulting in very limited corrections of the apparent ages (<2 ka). The only exception is the cement of 535B, which returned a $^{230}Th/^{232}Th$ ratio <5. There is a strong scattering in the apparent U-series age estimates: the enamel tissues both return much older results (>100 ka) compared with the other tissues, suggesting different uptake processes. Until these older results are confirmed to not result from a recent uranium leaching overprint, the more recent age estimates of 50–65 ka measured in dentine and cement should be considered as more reliable minimum age constraints for the fossil teeth.

Combined U-series and ESR age calculations. Radioelement concentrations obtained for the three sediment samples vary in a narrow range (0.3–11.1%; Table 3), showing the overall homogeneity the sediment surrounding the fossil specimen. In contrast, the limestone samples show more variability: one sample (D) returned concentration values by one order of magnitude higher than the other two (E and F). This suggests the presence of some impurities in the limestone or a contamination by sediment, which is why sample D was initially not considered for the dose rate evaluation. Mean radioelement concentration values were calculated for the sediment and limestone (Table 3). Given the position of the fossil specimen against the cave wall (Fig. 5), initial gamma dose rate evaluation was performed considering a 50% contribution from the sediment and another 50% from the cave wall.

The combination of U-series with ESR data does not return any finite age result with the US model. This indicates that some of the dental tissues have undergone uranium leaching. The use of the AU model and of a cement/enamel/dentine geometry return AU-ESR age results of 84 ± 6 ka and 105 ± 12 ka for 535A and 535B, respectively. Calculations indicate that the enamel of both samples has undergone significant uranium leaching, with a maximum past uranium concentration being up to *c.* 1.5-fold and *c.* 2.0-fold higher than today for 535A and 535B, respectively. In contrast, the other dental tissues show either slight (a few %) or no apparent uranium leaching. However, given the very low uranium concentrations measured in the tooth (<0.3 ppm), the weight of dental tissues in the total dose rate does not exceed 15%, including 11% from the enamel alone. Consequently, dentine and cement carry negligible weight in the total dose rate value. Although there is a significant uncertainty in the dose rate calculated for the enamel given the large amount of leaching modelled, it has only

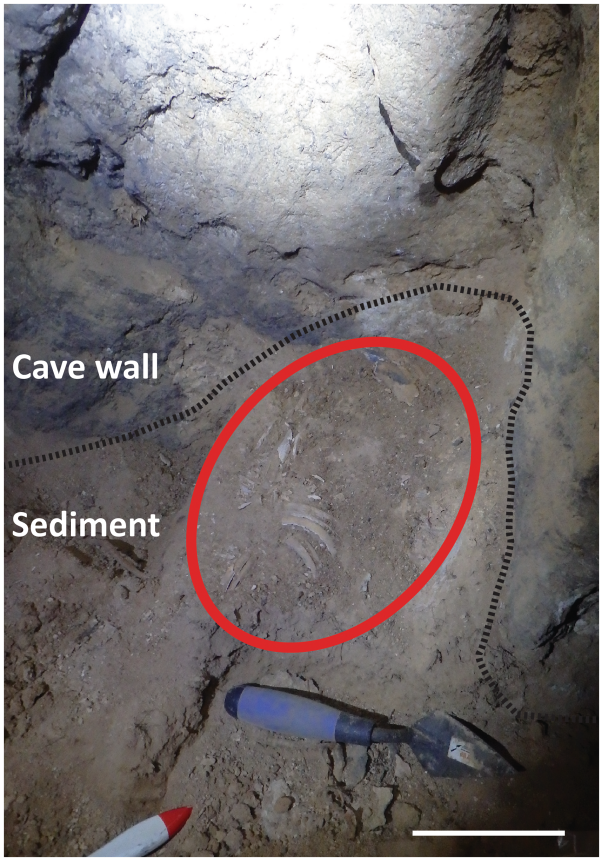

FIG. 5. Position of the fossil specimen (circled in red) in the field. The contact between the sediment and the cave wall is indicated by a dashed line. Scale bar represents 100 mm.

a very limited impact on the calculated age results. It does not make much difference whether the accelerating uptake, early uptake or linear uptake models are used given that the resulting age estimates vary by only 6–8 ka (Table 4).

Although there is a 27% difference in the D_E values obtained for the two samples, the calculated dose rates are virtually the same (Table 4). Although resulting age estimates differ by about 25%, they nevertheless agree at a 2σ confidence level.

We identify three main sources of uncertainty that might significantly affect the age results: (1) cement thickness; (2) water content in the sediment; and (3) gamma dose rate evaluation. Cement thickness was experimentally measured with digital callipers during sample preparation. A value of 0.3 mm was obtained, which indicates that it does contribute to only 50% (instead of the 100% initially assumed based on the infinite matrix assumption) of the beta dose rate from the external side of the enamel layer (Duval & Martin 2019). Refined calculations yield younger ages by 14% on average, resulting in estimates of 71 ± 5 ka and 92 ± 10 ka (Fig. 6). However, we acknowledge the existing uncertainty in thickness value, given that only one single measurement was performed. Assuming that cement thickness may significantly vary along the tooth, additional calculations were performed considering an associated error of ±0.2 mm. Resulting ages for a thickness of 0.1 (relative contribution, 25%; see Duval & Martin 2019) and 0.5 mm (relative contribution, 70%) are of 66 ± 5 ka and 75 ± 6 ka, respectively, for sample 535A. A similar calculation yields 85 ± 10 ka and 97 ± 11 ka, respectively, for sample 535B. In summary, age results may vary by 9–12 ka for a thickness variation of ±0.2 mm. This can most likely explain most of the existing age difference between the two samples from the same tooth, which were collected from different parts with variable associated cement thickness.

Dose rate evaluation was initially performed assuming a long-term water content of 15% (dry weight). It cannot be excluded that humidity in the cave has been much higher at some point in the past. With a water content multiplied by a factor of 2 (30%) for the sediment, AU-ESR age estimates become older by *c.* 17 ka, reaching 84 ± 7 and 109 ± 15 ka for samples 535A and 535B, respectively (Fig. 6). Regardless of the water content value considered between 10% and 30%, the ages of the two samples remain within Marine Isotope Stage 5 (130–71 ka; Lisiecki & Raymo 2005).

Finally, while initial gamma dose rate evaluation was performed using a reasonably conservative assumption based on an equal contribution from the sediment and limestone, we performed additional age calculations using an uncertainty of ±10% (Fig. 6). Resulting ages vary by −5 to +10 ka and −7 to +13 ka for samples 535A and 535B, respectively, and remain within 1σ agreement, indicating the limited impact of such uncertainty. When using radioelement concentrations from limestone sample D for dose rate calculation instead of a mean value from E and F (Table 3), the AU-ESR age of 535A becomes younger by *c.* 7 ka but remains nevertheless in good agreement with the initial calculations. In all cases, calculated age estimates remain correlated with the end of Marine Isotope Stage 5.

Phylogenetic analyses

Our maximum parsimony (Fig. 7) and undated Bayesian (Fig. 8) analyses recover topologies that are very similar to the equivalent analyses of Beck *et al.* (2020), which is unsurprising given that our morphological character matrix is only slightly modified from that previous study. Specifically, both analyses place Thylacoleonidae as sister to the remaining vombatiforms, with Phascolarctidae the next family to diverge (see also Beck *et al.* 2022). Within the remaining taxa, which collectively comprise

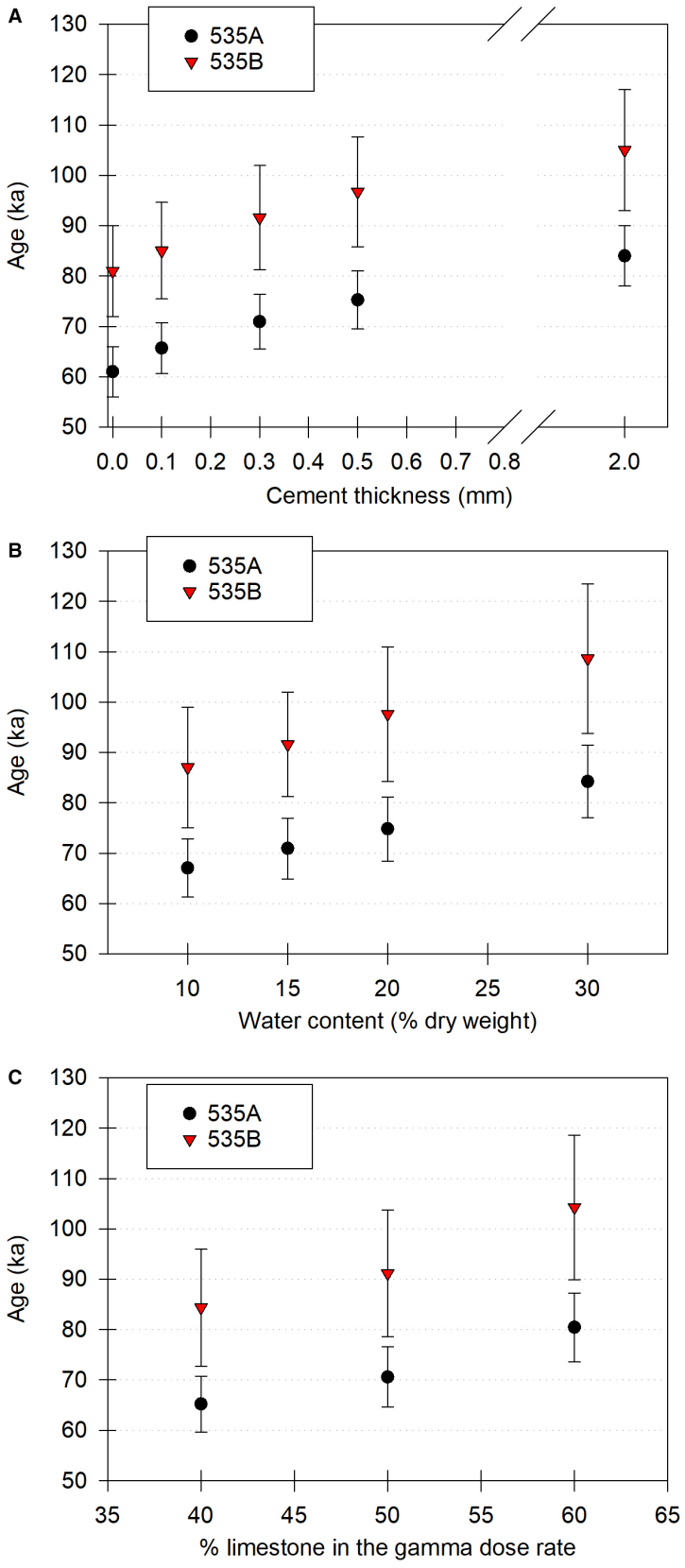

FIG. 6. Age sensitivity tests. A, age estimates vs cement thickness; 2 mm thickness corresponds to the infinite matrix conditions (100% of the beta dose rate from the external side of the enamel layer comes from the cement). B, age estimates vs long-term water content (% dry weight); accelerating uptake–electron spin resonance (AU-ESR) ages were calculated considering a cement thickness of 0.3 mm for both samples. C, age estimates vs contribution of limestone and/or sediment in the gamma dose rate evaluation; the AU-ESR ages were calculated considering a cement thickness of 0.3 mm for both samples.

FIG. 7. Maximum parsimony tree. Strict consensus of 392 most parsimonious trees (all of length 267) following maximum parsimony analysis of a 100 morphological character matrix focused on vombatiform relationships. Numbers at the nodes represent bootstrap values, based on 2000 bootstrap replicates with a maximum of 1000 trees saved per replicate.

Vombatomorphia *sensu* Beck *et al.* (2020), Vombatidae is sister to *Mukupirna* in both analyses, with this clade very strongly supported in the Bayesian analysis (BPP = 98%), but less so in the maximum parsimony analysis (bootstrap = 67%). Monophyly of Vombatidae also receives strong support in the Bayesian analysis (BPP = 91%), but again, less so in the maximum parsimony analysis (bootstrap = 60%). Within Vombatidae, both analyses find very strong support for a clade consisting of *Vombatus*, *Lasiorhinus*, *Ramsayia*, *Sedophascolomys* and *Phascolonus* (BPP = 100%; bootstrap = 96%), to the exclusion of the earlier branching *Nimbavombatus* and *Warendja*. Within this clade, both analyses find strong support for the monophyly of the giant vombatid genera *Ramsayia*, *Sedophascolomys* and *Phascolonus* (BPP = 100%; bootstrap = 88%). Under maximum parsimony the following four character state changes optimize as unambiguous synapomorphies of this clade: absence of enamel extending down the buccal surface of P3 and onto the root (char. 11, 1 → 0, consistency index (CI) = 0.5; note that this is a reversal of an unambiguous synapomorphy supporting *Mukupirna* + Vombatidae); incisive foramen located posteriorly (char. 43, 0 → 1, CI = 1); nasal aperture retracted to above cheek tooth row (char. 46, 1 → 2, CI = 0.429); and strongly arched bony palate present (char. 100, 0 → 1, CI = 1). The same four character state changes also optimize as unambiguous synapomorphies of this clade in the Bayesian analysis, but the consistency index for character 46 was slightly lower (CI = 0.375).

The Bayesian analysis indicates extremely weak support (BPP = 51%) for *Vombatus ursinus* and *V. hacketti* being sister to the giant vombatid clade, with *Lasiorhinus* outside this, but monophyly of *Vombatus* itself is not supported. The maximum parsimony analysis, meanwhile, recovered the giant vombatid clade in a polytomy with *Lasiorhinus* and *Vombatus ursinus* and *V. hacketti*, with the latter two taxa again not placed together in a single *Vombatus* clade. Within the giant vombatid clade, both analyses find moderate support for *Sedophascolomys* forming a clade with *Phascolonus* (BPP = 75%; bootstrap = 74%), to the exclusion of *Ramsayia*. In summary, both analyses strongly support the monophyly of giant vombatids but do not clearly resolve the relationships of this clade to *Vombatus* and *Lasiorhinus*.

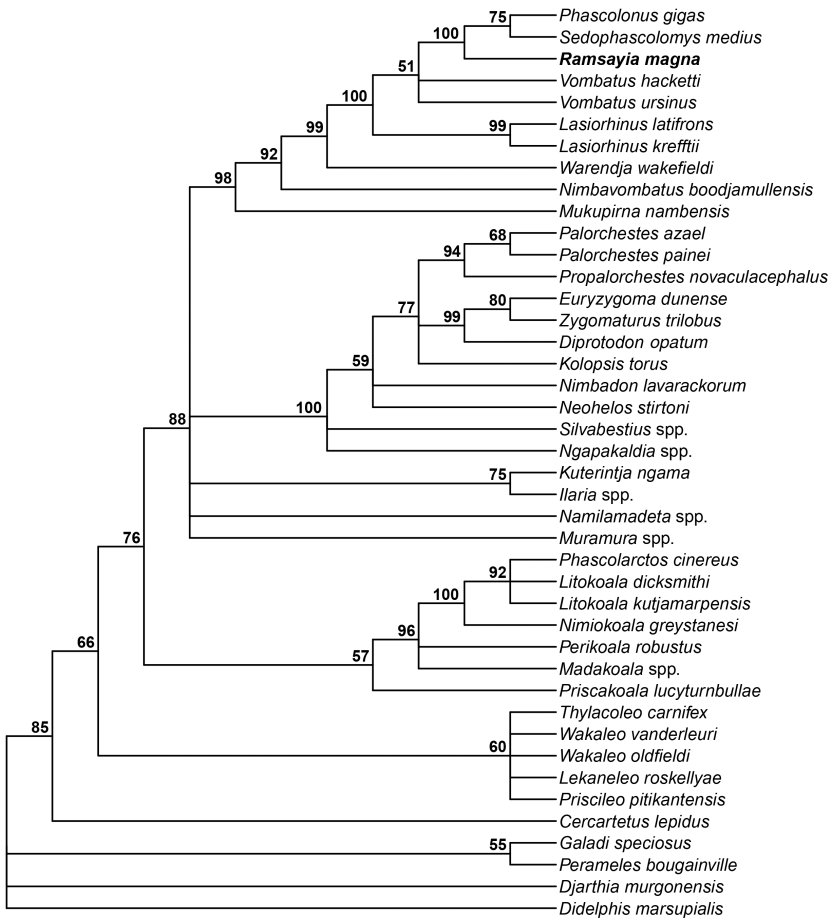

FIG. 8. Bayesian tree. A 50% majority rule consensus of post-burnin trees following undated Bayesian analysis of a 100 morphological character matrix focused on vombatiform relationships, assuming the Markov variable (Mk*v*) model. Numbers at the nodes represent Bayesian posterior probabilities, presented as percentages.

DISCUSSION

Anatomical adaptations

The resemblance of the premaxillary and upper incisor apparatus of *Ramsayia*, with its long, narrow and highly curved appearance, to those of giant castorine rodents such as *Trogontherium* and *Castoroides*, has been noted previously by Murray (1998), who hypothesized convergence in dietary preferences between these taxa. Two additional features well preserved in the new material of *Ramsayia magna* appear particularly noteworthy: the presence of a well-developed premaxillary 'spine' and potentially retracted nasals, and the development of large cranial sinuses. The median premaxillary spine (Bartholomai 1978; Murray 1991*b*, 1998), or premaxilla midline eminence (Trusler & Sharp 2016), is present and expressed to various degrees in many marsupials, including *Palorchestes azael* (Bartholomai 1978), *Diprotodon optatum* (Price 2008), *Hadronomas puckridgi* (Murray 1991*b*), *Phascolonus gigas* (Murray 1998), *Propalorchestes novaculacephalus* (Trusler & Sharp 2016) and, to a lesser extent, *Lasiorhinus latifrons* (Scott *et al.* 1988, fig. 3A). To the best of our knowledge, the functional anatomy of the median premaxillary spine in modern wombats has never been studied. Trusler & Sharp (2016) suggested that this crest in fossil marsupials (specifically in reference to *Palorchestes*) is analogous to that seen in some placentals, in which they can be formed by the premaxilla or maxilla and which are associated with retracted nasals, given that they provide structural support for the free portion of a cartilaginous nasal septum (Witmer *et al.* 1999). Although the nasals in QMF 60370 are poorly preserved, they appear to be significantly more retracted in *R. magna* than in modern wombat genera. To that end, they more superficially resemble the condition seen in *D. optatum*, a taxon thought to have possessed a large, fleshy nose (e.g. Archer 1984). A similar condition is likely to have occurred in *R. magna*.

The presence of large cranial sinuses within the parietal of some fossil marsupials was first noted by Owen (1870, 1877), and subsequently discussed by Klaauw (1931, 1946), Murray (1992), Black *et al.* (2010), Sharp (2016), Sharp & Rich (2016), Trusler & Sharp (2016) and Beck *et al.* (2022). Such parietal sinuses are present in a range of extinct large-bodied Vombatiformes, including

Nimbadon, *Neohelos*, *Silvabestius*, *Thylacoleo*, *Palorchestes*, *Kolopsis* and *Diprotodon*. However, this is the first time parietal sinuses have been recorded in a vombatid. We speculate here that the unusual 'dished-in'/depressed cranial roof of *Phascolonus gigas* (Murray 1998) may be because large sinuses are present in the parietals lateral to the endocranium, similar to those described here in *Ramsayia magna*, but not in the dorsal cranial roof, which may instead have the 'thickened' morphology seen in *Lasiorhinus* and *Vombatus* (Murray 1992); however, this requires confirmation.

Large cranial sinuses develop in response to an increase in skull size and accompanying temporalis muscles that cannot be accommodated by the inner table component of the neurocranial plate (Moss & Young 1960). The inner table responds instead to brain size (which decreases allometrically with increased skull size; Murray 1992; Sharp 2016) and grows independently of the other components of the neurocranial plate, namely the diploe and outer table. The outer table responds to the requirements of jaw adductor muscles, in particular the temporalis muscle, with the diploe intervening between the inner and outer tables. In moderately sized vombatids, such as the extant wombats, the development of a thickened diploe without sinus expansion is sufficient to accommodate their adductor muscles (Murray 1992); a similar condition can be observed in immature specimens of *Kolopsis* and *Neohelos* (Murray 1992; Black *et al*. 2010). In *Kolopsis*, pneumatization of the parietals becomes apparent when the M4 begins to emerge (Murray 1992), while in *Nimbadon*, frontal and squamosal sinuses are present in fully weaned individuals (stage IV), with parietal sinuses developed as a young adult (stage VI) (Black *et al*. 2010). The pneumatization of *R. magna*'s skull gives it a higher and more rounded appearance compared with the flattened skull of extant wombats, again, superficially convergent on the condition in *Diprotodon optatum*. Some digging mammals have broad heads that are used to displace or compact soils while burrowing (Hilderbrand 2013), and a similar function may also apply for modern wombats. If this is the case, it is unlikely that *R. magna*, with its higher and more rounded skull, was as fossorial as *Vombatus* or *Lasiorhinus*. Woolnough & Steele (2001) suggested that modern wombats approach the maximum body size for a burrowing mammal, supporting the idea that giant wombats were not burrowers. However, the body size argument is significantly weakened given that there are very large burrows in South America that were produced by >100 kg xenarthrans (Vizcaíno *et al*. 2001). A fossorial lifestyle in giant wombats could, however, be directly inferred using histological markers (Walker *et al*. 2020) if postcranial elements associated with identifiable cranial remains are recovered.

The well-developed parietal crests observed in *Ramsayia magna* further indicate a large area of attachment for the temporalis muscle and a relatively reduced masseter, the latter also indicated by the shallow infraorbital fossa. In modern wombats the masseter is larger in *Vombatus ursinus* than in *Lasiorhinus latifrons* (Nakajima & Townsend 1994; Sharp & Trusler 2015). Mastication in modern wombats consists of a high rate of powerful compressive strokes that can produce the extremely high occlusal forces necessary to masticate the grasses and sedges ingested (Murray 1998). Compared with kangaroos, wombats generate higher bite forces by increasing the amounts of working side musculature (Crompton *et al*. 2008). In *L. latifrons* the relatively larger temporalis and relatively smaller masseter relative to *V. ursinus* have been associated with narrower horizontal movements and higher vertical bite forces in the former taxon in response to a higher fibre diet (Sharp & Trusler 2015). The likely presence of large temporalis muscles in *Ramsayia*, suggested by its sinus development and parietal crests, implies that it also utilized high biting forces. This, together with what is probably a relatively smaller masseter, suggests that it may have had an even higher fibre diet than does *L. latifrons*, congruent with the general observation that larger herbivorous mammals feed on lower quality vegetation (the Jarman–Bell principle; Müller *et al*. 2013).

Qualitative and quantitative examination of the function of endocranial sinuses in vombatiforms consistently suggests that they provide an area for the attachment of larger temporalis muscles without the need to develop sagittal crests, thereby increasing mechanical efficiency and lightening the skull (Murray 1992; Sharp & Rich 2016). They may also serve to dissipate stress more evenly, posteriorly away from the nasal region, which may be more prone to failure under very high or repetitive bite forces (Tanner *et al*. 2008; Sharp & Rich 2016). Such biomechanical adaptations would clearly be advantageous for *Ramsayia*, a large vombatid with large temporalis muscles and high-frequency mastication cycles, by reducing fatigue failure caused by repetitive stress (Figueirido *et al*. 2014; Sharp & Rich 2016).

Age, geographic range and extinction

Direct dating of the *Ramsayia magna* specimen described here yielded AU-ESR age estimates of 71 ± 5 and 92 ± 10 ka, respectively, for the two samples collected from the same tooth (Table 4). The age discrepancy is most likely to be due to some lateral variations of the cement thickness. While we acknowledge the existing uncertainty around the long-term water content and the evaluation of the gamma dose rate, our sensitivity tests

show that the resulting ages remain consistently in Marine Isotope Stage 5 (Fig. 6), and a mean age of 81 ± 15 ka may be proposed for the fossil specimen. This age represents the first direct date for *R. magna*, and thus also the last appearance datum for this taxon. *Ramsayia* has previously been argued to have gone extinct alongside other megafauna primarily due to human colonization in the Late Pleistocene (Johnson 2002; Bartlett *et al.* 2016), despite having had no directly dated records (Wroe *et al.* 2013; Price *et al.* 2018). Even with the new date reported here, given the paucity of temporal, spatial, palaeobiological and palaeoecological information, speculation on the cause of the extinction of *R. magna* is premature. This specimen also represents the most northerly confirmed record of this taxon, although a mandibular specimen from Leafy Tree Cave, Mungana, near Chillagoe in north Queensland (QMF 31671), examined in the course of the current study, can also be tentatively referred to this taxon based on its size, highly fragmented but probably subtriangular left p3, and a narrow i1. The addition of central and northern Queensland records to this species indicates that *R. magna* ranged from tropical to temperate environments.

Evolutionary relationships

Phylogenetic analysis using maximum parsimony and Bayesian inference of a 100 morphological character matrix (80 craniodental, 20 postcranial) intended to resolve relationships within Vombatiformes strongly supports the monophyly of a clade consisting of the giant vombatids *Ramsayia*, *Sedophascolomys* and *Phascolonus*. This clade is supported by four unambiguous synapomorphies, two of which, a posteriorly located incisive foramen (char. 43) and presence of a strongly arched bony palate (char. 100), show zero homoplasy. Murray (1998) proposed that the evolution of large body sizes in wombats was a response to nutrient poor, highly fibrous foods and due to the increasing aridification of the continent throughout the late Neogene and Quaternary. Specializations in the giant wombats, particularly evident in their incisor anatomy, were suggested by Murray (1998) to be related to further partitioning of grazing resources. Our recovery of a single giant vombatid clade suggests that the move towards larger body sizes, if in response to lower quality food, occurred before any of the specializations associated with niche partitioning of the grazing landscape.

The relationship of the giant vombatid clade to the modern genera *Lasiorhinus* and *Vombatus* was not clearly resolved. By contrast, Tedford (2002) presented a maximum parsimony analysis of 16 craniodental characters that placed *Lasiorhinus* as sister to the same giant vombatid clade found here (Tedford 2002, fig. 7). However, of these 16 characters, we found that we could consistently score only four of them (these have been included in our analysis); we found the remainder to be unclearly defined or to show continuous variation that could not be easily parsed into discrete states (see Supporting Information and Louys *et al.* 2022*b*). In the latter was the presence or absence of a premaxillary 'spine', although we acknowledge that the presence of a particularly well-developed 'spine' is a distinctive feature of *Ramsayia* (see comments above). Other studies that have used versions of Tedford's (2002) characters have scored some of them quite differently (e.g. Murray 1998; Brewer *et al.* 2015, 2018), suggesting that they are indeed difficult to score consistently, as we found here. We also note that the character scores in table 1 of Tedford (2002) are inconsistent with the accompanying text describing their distribution in vombatids and other vombatiforms (we suspect, but cannot be sure, that the column labelled '*Lasiorhinus*' in fact represents *Ramsayia magna*, and vice versa), which makes direct comparison difficult.

Although our phylogenetic results persuade us that *Ramsayia*, *Sedophascolomys* and *Phascolonus* do indeed form a clade, resolution of the relationship of this clade to *Lasiorhinus* and *Vombatus* (and also the relationship of the extinct *V. hacketti* to the living *V. ursinus*; see Murray 1998, pp. 21–22) will require additional data. Discovery of additional postcranial remains may prove informative given that *Vombatus* and *Lasiorhinus* show a number of postcranial differences (Scott & Richardson 1987*a*, 1987*b*; Murray 1998). Postcranial material is available for *Phascolonus gigas* (Stirling 1913; Murray 1998) but as yet not for *Ramsayia* or *Sedophascolomys*. Given that representatives of all three giant genera are known from Plio-Pleistocene deposits, they would also seem to be obvious candidates for palaeoproteomic studies (Buckley 2018; Peters *et al.* 2021), which may convincingly resolve their precise relationship to living wombats.

CONCLUSION

The partial skull recovered from Lower Johansons Cave, Rockhampton, Queensland, can be attributed to the giant wombat *Ramsayia magna*. These remains represent the most complete cranial material of this species and preserve traits not previously observed for this taxon and the family. The presence of a parietal sinus indicates that some members of the Vombatidae underwent cranial pneumatization due to increases in body size, a condition also seen in other extinct giant marsupial species but not previously recorded for

vombatids. The larger body and cranial sizes were probably a response to increases in the volume of poorer quality plants ingested. The presence of a well-developed premaxillary spine suggests that *R. magna* possessed a large fleshy nose, and superficially may have resembled the diprotodontid *Diprotodon optatum*. Our phylogenetic analysis indicates that gigantism in wombats, defined here as attaining a body mass greater than 70 kg, evolved only once, and that it preceded the unusual cranial grazing adaptations displayed by members of the clade. The partial skull is dated to *c*. 80 000 years ago, which represents the only securely dated fossil specimen of this species. Reasons for its eventual extinction cannot be determined based on current data.

Acknowledgements. This specimen was collected under Queensland Government Department of Environment and Science permit PTU19-002298, issued to GJP under s9(1)(a) Nature Conservation (Administration) Regulation 2017 Permit to Take, Use, Keep or Interfere with Cultural or Natural Resources. We thank Pip Brewer for her insightful comments and discussion on this specimen, and on wombat evolution and taxonomy more generally. MD is grateful to María Jesús Alonso Escarza, CENIEH, for technical support throughout the analytical procedure. MD is the recipient of a Ramón y Cajal Fellowship (RYC2018-025221-I) funded by MCIN/AEI/10.13039/501100011033 and by 'ESF Investing in your future'. We thank Gavin Prideaux and an anonymous reviewer, and editor Sally Thomas, for their helpful and constructive comments. Open access publishing facilitated by Griffith University, as part of the Wiley - Griffith University agreement via the Council of Australian University Librarians.

Author contributions. **Conceptualization** J Louys (JL), GJ Price (GJP); **Data Curation** M Duval (MD), RMD Beck (RMDB); **Formal Analysis** JL, MD, RMDB; **Funding Acquisition** GJP; **Investigation** JL, MD, RMDB, E Pease (EP), I Sobbe (IS), N Sands, GJP; **Methodology** JL, MD, RMDB; **Project Administration** GJP; **Resources** MD, IS, GJP; **Software** MD, RMDB; **Supervision** GJP; **Visualization** JL, MD, RMDB, EP, GJP; **Writing – Original Draft Preparation** JL, MD, RMDB; **Writing – Review & Editing** JL, MD, RMDB, IS, GJP.

DATA ARCHIVING STATEMENT

Photogrammetry image series (https://doi.org/10.17602/M2/M461723 (internal view); https://doi.org/10.17602/M2/M461634 (external view)) and 3D models (https://doi.org/10.17602/M2/M461726 (internal); https://doi.org/10.17602/M2/M461637 (external)) of QMF 60370 are available in MorphoSource (https://www.morphosource.org/projects/000455063). Phylogenetic data are archived in MorphoBank (http://morphobank.org/permalink/?P4316). Data also archived in the Dryad Digital Repository (https://doi.org/10.5061/dryad.tmpg4f520).

Editor. Lionel Hautier

SUPPORTING INFORMATION

Additional Supporting Information can be found online (https://doi.org/10.1002/spp2.1475):

Appendix S1. 3D model of *Ramsayia magna*.

Appendix S2. Nexus file.

Appendix S3. Comments on the morphological characters and scorings used by Tedford (2002) to resolve vombatid phylogeny.

REFERENCES

ARCHER, M. 1976. Bluff Downs Local Fauna. *In* Archer, M. and Wade, M. Results of the Ray E. Lemley Expeditions, Part I. The Allingham Formation and a new Pliocene vertebrate fauna from northern Queensland. *Memoirs of the Queensland Museum*, **17**, 379–397.

ARCHER, M. 1984. The Australian marsupial radiation. 633–808. *In* ARCHER, M. and CLAYTON, G. (eds) *Vertebrate zoogeography and evolution in Australasia*. Hesperian Press, 1203 pp.

BARTHOLOMAI, A. 1978. The rostrum in *Palorchestes* Owen (Marsupialia: Diprotodontidae). *Memoirs of the Queensland Museum*, **18**, 145–149.

BARTLETT, L. J., WILLIAMS, D. R., PRESCOTT, G. W., BALMFORD, A., GREEN, R. E., ERIKSSON, A., VALDES, P. J., SINGARAYER, J. S. and MANICA, A. 2016. Robustness despite uncertainty: regional climate data reveal the dominant role of humans in explaining global extinctions of Late Quaternary megafauna. *Ecography*, **39**, 152–161.

BECK, R. M. D., LOUYS, J., BREWER, P., ARCHER, M., BLACK, K. H. and TEDFORD, R. H. 2020. A new family of diprotodontian marsupials from the latest Oligocene of Australia and the evolution of wombats, koalas, and their relatives (Vombatiformes). *Scientific Reports*, **10**, 9741.

BECK, R. M. D., VOSS, R. and JANSA, S. 2022. Craniodental morphology and phylogeny of marsupials. *Bulletin of the American Museum of Natural History*, **457**, 1–350.

BLACK, K. H., ARCHER, M., HAND, S. J. and GODTHELP, H. 2010. First comprehensive analysis of the cranial ontogeny in a fossil marsupial—from a 15-million-year-old cave deposit in northern Australia. *Journal of Vertebrate Paleontology*, **30**, 993–1011.

BREWER, P., ARCHER, M., HAND, S. J. and ABEL, R. 2015. New genus of primitive wombat (Vombatidae, Marsupialia) from Miocene deposits in the Riversleigh World Heritage

area (Queensland, Australia). *Palaeontologia Electronica*, **18**, 1–40.

BREWER, P., ARCHER, M., HAND, S. and PRICE, G. J. 2018. A new species of Miocene wombat (Marsupialia, Vombatiformes) from Riversleigh, Queensland, Australia, and implications for the evolutionary history of the Vombatidae. *Palaeontologia Electronica*, **21**, 1–48.

BUCKLEY, M. 2018. Paleoproteomics: an introduction to the analysis of ancient proteins by soft ionisation mass spectrometry. 31–52. *In* LINDQVIST, C. and RAJORA, O. P. (eds) *Paleogenomics*. Springer, 427 pp.

BURNETT, G. T. 1830. Illustrations of the Quadrupeda, or quadrupeds; being the arrangement of the true four-footed beasts indicated in outline. *Quarterly Journal of Science, Literature & Art*, **28**, 336–353.

CLARK, T. R., ROFF, G., ZHAO, J.-X., FENG, Y.-X., DONE, T. J. and PANDOLFI, J. M. 2014. Testing the precision and accuracy of the U–Th chronometer for dating coral mortality events in the last 100 years. *Quaternary Geochronology*, **23**, 35–45.

CROMPTON, A. W., LIEBERMAN, D. E., OWERKOWICZ, T., BAUDINETTE, R. V. and SKINNER, J. 2008. Motor control of masticatory movements in the southern hairy-nosed wombat (*Lasiorhinus latifrons*). 83–111. *In* VINYARD, C. J., RAVOSA, M. J. and WALL, C. E. (eds) *Primate craniofacial function and biology*. Springer, 328 pp.

DAWSON, L. 1981. The status of the taxa of extinct giant wombats (Vombatidae: Marsupialia), and a consideration of vombatid phylogeny. *Australian Mammalogy*, **4**, 65–79.

DAWSON, L. 1983. On the uncertain generic status and phylogenetic relationships of the large, extinct vombatid species *Phascolomys medius* Owen 1872 (Marsupialia, Vombatidae). *Australian Mammalogy*, **6**, 5–14.

DE SANTIS, L. R., FIELD, J. H., WROE, S. and DODSON, J. R. 2017. Dietary responses of Sahul (Pleistocene Australia–New Guinea) megafauna to climate and environmental change. *Paleobiology*, **43**, 181–195.

DUVAL, M. and GRÜN, R. 2016. Are published ESR dose assessments on fossil tooth enamel reliable? *Quaternary Geochronology*, **31**, 19–27.

DUVAL, M. and MARTIN, L. 2019. An application of DosiVox to ESR dating of fossil teeth: evaluating the impact of dental tissue thickness on the external beta dose rate evaluation. *Geochronometria*, **46**, 102–110.

DUVAL, M. and MARTÍN-FRANCÉS, L. 2017. Quantifying the impact of μCT-scanning of human fossil teeth on ESR age results. *American Journal of Physical Anthropology*, **163**, 205–212.

DUVAL, M., WESTAWAY, K., ZAIM, Y., RIZAL, Y., ASWAN, PUSPANINGRUM, M. R., TRIHASCARYO, A., ALBERS, P. C. H., SMITH, H. E., DRAWHORN, G. M., PRICE, G. J. and LOUYS, J. 2021. New chronological constraints for the Late Pleistocene fossil assemblage and associated breccia from Ngalau Sampit, Sumatra. *Open Quaternary*, **7**, 1–24.

FIGUEIRIDO, B., TSENG, Z. J. and SERRANO-ALARCÓN, F. J. 2014. Three-dimensional computer simulations of feeding behaviour in red and giant pandas relate skull biomechanics with dietary niche partitioning. *Biology Letters*, **10**, 20140196.

GRÜN, R. 2000. Methods of dose determination using ESR spectra of tooth enamel. *Radiation Measurements*, **32**, 767–772.

GRÜN, R. 2009. The DATA program for the calculation of ESR age estimates on tooth enamel. *Quaternary Geochronology*, **4**, 231–232.

GRÜN, R. and KATZENBERGER-APEL, O. 1994. An alpha irradiator for ESR dating. *Ancient TL*, **12**, 35–38.

GRÜN, R., SCHWARCZ, H. P. and CHADAM, J. 1988. ESR dating of tooth enamel: coupled correction for U-uptake and U-series disequilibrium. *International Journal of Radiation Applications & Instrumentation D: Nuclear Tracks & Radiation Measurements*, **14**, 237–241.

GUÉRIN, G., MERCIER, N. and ADAMIEC, G. 2011. Dose-rate conversion factors: update. *Ancient TL*, **29**, 5–8.

HARRISON, L. B. and LARSSON, H. C. E. 2015. Among-character rate variation distributions in phylogenetic analysis of discrete morphological characters. *Systematic Biology*, **64**, 307–324.

HILDEBRAND, M. 2013. Digging of quadrupeds. 89–109. *In* HILDEBRAND, M., BRAMBLE, D. M., LIEM, K. F. and WAKE, D. B. (eds) *Functional vertebrate morphology*. Harvard University Press, 430 pp.

HOCKNULL, S. A. 2009. Late Cainozoic rainforest vertebrates from Australopapua: evolution, biogeography and extinction. PhD thesis, University of New South Wales.

HOCKNULL, S. A., LEWIS, R., ARNOLD, L. J., PIETSCH, T., JOANNES-BOYAU, R., PRICE, G. J., MOSS, P., WOOD, R., DOSSETO, A., LOUYS, J., OLLEY, J. and LAWRENCE, R. A. 2020. Extinction of eastern Sahul megafauna coincides with sustained environmental deterioration. *Nature Communications*, **11**, 2250.

JOHNSON, C. N. 2002. Determinants of loss of mammal species during the Late Quaternary 'megafauna' extinctions: life history and ecology, but not body size. *Proceedings of the Royal Society B*, **269**, 2221–2227.

KIRSCH, J. A. W. 1968. Prodromus of the comparative serology of Marsupialia. *Nature*, **217**, 418–420.

KLAAUW, C. J. V. D. 1931. The auditory bulla in some fossil mammals: with a general introduction to this region of the skull. *Bulletin of the American Museum of Natural History*, **62**, 1–352.

KLAAUW, C. J. V. D. 1946. Cerebral skull and facial skull. *Archives Néerlandaises de Zoologie*, **1**, 16–37.

KUPCZIK, K., SHARP, A. C. and TRUSLER, P. W. 2015. Morphology of the jaw-closing musculature in the common wombat (*Vombatus ursinus*) using digital dissection and magnetic resonance imaging. *PLoS One*, **10**, e0117730.

LEWIS, P. O. 2001. A likelihood approach to estimating phylogeny from discrete morphological character data. *Systematic Biology*, **50**, 913–925.

LISIECKI, L. E. and RAYMO, M. E. 2005. A Pliocene–Pleistocene stack of 57 globally distributed benthic $\delta^{18}O$ records. *Paleoceanography*, **20**, PA1003.

LOUYS, J. 2015. Wombats (Vombatidae: Marsupialia) from the Pliocene Chinchilla Sand, southeastern Queensland, Australia. *Alcheringa*, **39**, 394–406.

LOUYS, J., DUVAL, M., BECK, R. M. D., PEASE, E., SOBBE, I., SANDS, N. and PRICE, G. J. 2022*a*. Data from: Cranial remains of *Ramsayia magna* from the Late Pleistocene of Australia and the evolution of gigantism in wombats (Vombatidae; Marsupialia). *Dryad Digital Repository*. https://doi.org/10.5061/dryad.tmpg4f520

LOUYS, J., DUVAL, M., BECK, R. M. D., PEASE, E., SOBBE, I., SANDS, N. and PRICE, G. J. 2022*b*. Project 4316: Cranial remains of *Ramsayia magna* from the Late Pleistocene of Australia and the evolution of gigantism in wombats (Vombatidae; Marsupialia). *Morphobank*. http://morphobank.org/permalink/?P4316

MAHONEY, J. A. and RIDE, W. D. L. 1975. Index to the genera and species of fossil Mammalia described from Australia and New Guinea between 1838 and 1968. *Western Australian Museum Special Publication*, **6**, 1–250.

MARSH, R. E. 1999. Beta-gradient isochrons using electron paramagnetic resonance: towards a new dating method in archaeology. MSc thesis, McMaster University.

McNAMARA, G. C. 1990. The Wyandotte local fauna: a new, dated, Pleistocene vertebrate fauna from northern Queensland. *Memoirs of the Queensland Museum*, **28**, 285–297.

MOSS, M. L. and YOUNG, R. W. 1960. A functional approach to craniology. *American Journal of Physical Anthropology*, **18**, 281–292.

MÜLLER, D. W. H., CODRON, D., MELORO, C., MUNN, A., SCHWARM, A., HUMMEL, J. and CLAUSS, M. 2013. Assessing the Jarman–Bell Principle: scaling of intake, digestibility, retention time and gut fill with body mass in mammalian herbivores. *Comparative Biochemistry & Physiology A: Molecular & Integrative Physiology*, **164**, 129–140.

MURIE, J. 1866. On the identity of the hairy-nosed wombat (*Phascolomys lasiorhinus*, Gould) with the broad-fronted wombat (*P. latifrons*, Owen), with further observations on the several species of this genus. *Proceedings of the Zoological Society of London*, **1865**, 838–854.

MURRAY, P. 1991*a*. The Pleistocene megafauna of Australia. 1070–1164. *In* VICKERS-RICH, P., MONAGHAN, J. M., BAIRD, R. F. and RICH, T. H. (eds) *Vertebrate palaeontology of Australasia*. Pioneer Design Studies, 1437 pp.

MURRAY, P. 1991*b*. The sthenurine affinity of the late Miocene kangaroo, *Hadronomas puckridgi* Woodburne (Marsupialia, Macropodidae). *Alcheringa*, **15**, 255–283.

MURRAY, P. F. 1992. Thinheads, thickheads and airheads: functional craniology of some diprotodontan marsupials. *The Beagle: Records of the Museums & Art Galleries of the Northern Territory*, **9**, 71–87.

MURRAY, P. F. 1998. Palaeontology and palaeobiology of wombats. 1–33. *In* WELLS, R. T. and PRIDMORE, P. A. (eds) *Wombats*. Surrey, Beatty & Sons, 332 pp.

MYERS, T. J. 2001. Prediction of marsupial body mass. *Australian Journal of Zoology*, **49**, 99–118.

NAKAJIMA, K. and TOWNSEND, G. 1994. A morphometric study of the skulls of two species of wombats (*Vombatus ursinus* and *Lasiorhinus latifrons*). *Australian Mammalogy*, **17**, 65–72.

O'REILLY, J. E. and DONOGHUE, P. C. J. 2018. The efficacy of consensus tree methods for summarizing phylogenetic relationships from a posterior sample of trees estimated from morphological data. *Systematic Biology*, **67**, 354–362.

OWEN, R. 1858. Professor Owen's lecture on Monday evening. *The Leeds Mercury*, **95** (6852). 28 September, 1858.

OWEN, R. 1866. *On the anatomy of vertebrates*, **2**. Longmans, Green, London.

OWEN, R. 1870. On the fossil mammals of Australia. Part III. *Diprotodon australis*, Owen. *Philosophical Transactions of the Royal Society of London*, **160**, 519–578.

OWEN, R. 1872. On the fossil mammals of Australia. Part VII. Genus *Phascolomys*; species exceeding the existing ones in size. *Philosophical Transactions of the Royal Society of London*, **162**, 241–258.

OWEN, R. 1877. *On the fossil mammals of Australia, with a notice of the extinct marsupials of England*. J. Erxleben, London.

PETERS, C., RICHTER, K. K., MANNE, T., DORTCH, J., PATERSON, A., TRAVOUILLON, K., LOUYS, J., PRICE, G. J., PETRAGLIA, M., CROWTHER, A. and BOIVIN, N. 2021. Species identification of Australian marsupials using collagen fingerprinting. *Royal Society Open Science*, **8**, 211229.

PRICE, G. J. 2008. Taxonomy and palaeobiology of the largest-ever marsupial, *Diprotodon* Owen 1838 (Diprotodontidae, Marsupialia). *Zoological Journal of the Linnean Society*, **153**, 389–417.

PRICE, G. J. 2022. 3D model of *Ramsayia magna* skull (QMF60370) (Vomabatidae; Marsupialia) from the Pleistocene of Australia. *MorphoSource*. https://www.morphosource.org/projects/000455063

PRICE, G. J., ZHAO, J. X., FENG, Y. X. and HOCKNULL, S. A. 2009. New U/Th ages for Pleistocene megafauna deposits of southeastern Queensland, Australia. *Journal of Asian Earth Sciences*, **34**, 190–197.

PRICE, G. J., FENG, Y. X., ZHAO, J. X. and WEBB, G. E. 2013. Direct U–Th dating of vertebrate fossils with minimum sampling destruction and application to museum specimens. *Quaternary Geochronology*, **18**, 1–8.

PRICE, G. J., LOUYS, J., FAITH, J. T., LORENZEN, E. and WESTAWAY, M. C. 2018. Big data little help in megafauna mysteries. *Nature*, **558**, 23–25.

SCOTT, G. G. and RICHARDSON, K. C. 1987*a*. Osteological differences of the axial skeleton between *Lasiorhinus latifrons* (Owen 1845) and *Vombatus ursinus* (Shaw 1800) (Marsupialia: Vombatidae). *Records of the South Australian Museum*, **22**, 29–39.

SCOTT, G. G. and RICHARDSON, K. C. 1987*b*. Appendicular osteological differences between *Lasioruinus latifrons* (Owen, 1845) and *Vombatus ursinus* (Shaw, 1800) (Marsupialia: Vombatidae). *Records of the South Australian Museum*, **22**, 95–102.

SCOTT, G. G., RICHARDSON, K. C. and GROVES, C. P. 1988. Osteological differences of the skulls of *Lasiorhinus latifrons* Owen, 1845 and *Vombatus ursinus* Shaw, 1800 (Marsupialia, Vombatidae). *Australian Journal of Zoology*, **36**, 599–609.

SHAO, Q., BAHAIN, J.-J., FALGUÈRES, C., DOLO, J.-M. and GARCIA, T. 2012. A new U-uptake model for

combined ESR/U-series dating of tooth enamel. *Quaternary Geochronology*, **10**, 406–411.

SHAO, Q., BAHAIN, J. J., DOLO, J. M. and FALGUÈRES, C. 2014. Monte Carlo approach to calculate US-ESR age and age uncertainty for tooth enamel. *Quaternary Geochronology*, **22**, 99–106.

SHARP, A. C. 2016. A quantitative comparative analysis of the size of the frontoparietal sinuses and brain in vombatiform marsupials. *Memoirs of Museum Victoria*, **74**, 331–342.

SHARP, A. C. and RICH, T. H. 2016. Cranial biomechanics, bite force and function of the endocranial sinuses in *Diprotodon optatum*, the largest known marsupial. *Journal of Anatomy*, **228**, 984–995.

SHARP, A. C. and TRUSLER, P. W. 2015. Morphology of the jaw-closing musculature in the common wombat (*Vombatus ursinus*) using digital dissection and magnetic resonance imaging. *PloS One*, **10**, e0117730.

STIRLING, E. 1913. On the identity of *Phascolomys* (*Phascolonus*) *gigas* Owen and *Sceparnodon ramsayi* Owen with a description of some parts of its skeleton. *Memoirs of the Royal Society of South Australia*, **1**, 127–178.

TANNER, J. B., DUMONT, E. R. and SAKAI, S. T. 2008. Of arcs and vaults: the biomechanics of bone-cracking in spotted hyenas (*Crocuta crocuta*). *Biological Journal of the Linnean Society*, **95**, 246–255.

TEDFORD, R. H. 2002. The basicranium of the giant wombat *Phascolonus gigas* Owen (Vombatidae: Marsupialia) and its significance in phylogeny. *Smithsonian Contributions to Paleobiology*, **93**, 39–47.

TEDFORD, R. H. and WELLS, R. T. 1990. Pleistocene deposits and fossil vertebrates from the "Dead Heart of Australia". *Memoirs of the Queensland Museum*, **28**, 263–284.

TEDFORD, R. H., WELLS, R. T. and PRIDEAUX, G. J. 2006. Pliocene and earlier Pleistocene marsupial evolution in southeastern Australia. *Alcheringa*, **30**, 313–322.

TRUSLER, P. W. and SHARP, A. C. 2016. Description of new cranial material of *Propalorchestes* (Marsupialia: Palorchestidae) from the middle Miocene Camfield Beds, Northern Territory, Australia. *Memoirs of Museum Victoria*, **74**, 291–324.

TURNBULL, W. D., LUNDELIUS, E. L. Jr and TEDFORD, R. H. 1990. Fossil mammals of the Coimadai Local Fauna near Bacchus Marsh, Victoria. *Memoirs of the Queensland Museum*, **28**, 223–245.

VIZCAÍNO, S. F., ZÁRATE, M., BARGO, M. S. and DONDAS, A. 2001. Pleistocene burrows in the Mar del Plata area [Argentina] and their probable builders. *Acta Palaeontologica Polonica*, **46**, 289–301.

WALKER, M. M., LOUYS, J., HERRIES, A. I. R., PRICE, G. J. and MISZKIEWICZ, J. J. 2020. Humerus midshaft histology in a modern and fossil wombat. *Australian Mammalogy*, **43**, 30–39.

WITMER, L. M., SAMPSON, S. D. and SOLUNIAS, N. 1999. The proboscis of tapirs (Mammalia: Perissodactyla): a case study in novel narial anatomy. *Journal of Zoology*, **249**, 249–267.

WOODBURNE, M. O. 1984. Families of marsupials: relationships, evolution and biogeography. *Series in Geology, Notes for Short Course*, **8**, 48–71.

WOOLNOUGH, A. P. and STEELE, V. R. 2001. The palaeoecology of the Vombatidae: did giant wombats burrow? *Mammal Review*, **31**, 33–45.

WROE, S., FIELD, J. H., ARCHER, M., GRAYSON, D. K., PRICE, G. J., LOUYS, J., FAITH, J. T., WEBB, G. E. and MOONEY, S. D. 2013. Climate change frames debate over the extinction of megafauna in Sahul (Pleistocene Australia-New Guinea). *Proceedings of the National Academy of Sciences USA*, **110**, 8777–8781.

ZHAO, J.-X., YU, K.-F. and FENG, Y.-X. 2009. High-precision ^{238}U–^{234}U–^{230}Th disequilibrium dating of the recent past: a review. *Quaternary Geochronology*, **4**, 423–433.